ELSEVIER

Surface Science 439 (1999) 59–72

surface science

www.elsevier.nl/locate/susc

Morphology, surface core-level shifts and surface energy of the faceted GaAs(112)A and ($\bar{1}\bar{1}\bar{2}$)B surfaces

K. Jacobi [a,*], J. Platen [a], C. Setzer [a], J. Márquez [a], L. Geelhaar [a], C. Meyne [b], W. Richter [b], A. Kley [a], P. Ruggerone [c], M. Scheffler [a]

[a] *Fritz-Haber-Institut der Max-Planck-Gesellschaft, Faradayweg 4- 6, D-14195 Berlin, Germany*
[b] *Institut für Festkörperphysik, Technische Universität Berlin, Hardenbergstraße36, D-10623 Berlin, Germany*
[c] *Istituto Nazionale per la Fisica della Materia - Dipartimento di Fisica, UniversitádiCagliari, I-09042 Monserrato (CA), Italy*

Received 26 April 1999; accepted for publication 20 May 1999

Abstract

The GaAs(112)A and ($\bar{1}\bar{1}\bar{2}$)B surfaces have been prepared by molecular-beam epitaxy (MBE) and analyzed in situ by low-energy electron diffraction (LEED) and surface core-level spectroscopy of the Ga 3d and As 3d core levels using synchrotron radiation. The morphology of these surfaces has been studied in situ by scanning tunneling microscopy (STM) and ex situ by scanning electron microscopy (SEM) and atomic force microscopy (AFM). Neither of the surfaces is stable, but both decompose into facets under standard MBE preparation conditions. The (112)A surface is covered by regular depressions (inverted pyramids) with a pentagonal base and with side walls formed of low-energy (111), {110}, and as yet unobserved {124} facets. The ($\bar{1}\bar{1}\bar{2}$)B surface exhibits depressions with ($\bar{1}\bar{1}\bar{1}$), {$0\bar{1}\bar{1}$}, and ($\bar{1}\bar{1}\bar{3}$) facets on a rectangular base. These results are in agreement with ab-initio calculations of surface energies based on density functional theory. The theoretical findings show that, by forming roof-like structures employing {110} or {111} and {113} surfaces, the surface free energy can be lowered below the values found for a large number of reasonable GaAs(112)A and ($\bar{1}\bar{1}\bar{2}$)B model surfaces.

Keywords: Atomic force microscopy; Density functional calculations; Gallium arsenide; High-index single crystal surfaces; Low-energy electron diffraction (LEED); Low-index single crystal surfaces; Molecular beam epitaxy; Scanning electron microscopy (SEM); Scanning tunneling microscopy; Single crystal surfaces; Surface energy; Surface structure, morphology, roughness, and topography; Synchrotron radiation photoelectron spectroscopy

1. Introduction

Semiconductor quantum dots have attracted an increasing amount of interest recently [1]. Quantum dots consist of some 10^4 atoms and cannot be prepared by lithography techniques; instead, strain-induced self-assembly of small islands has been successfully used to produce, for example, small InAs islands within a GaAs matrix grown on a GaAs(100) surface. The current understanding of this process is as follows. Since the lattice mismatch between InAs and GaAs amounts to 7%, only the first 1.5 monolayers of InAs grow pseudomorphically on GaAs(100). For greater thicknesses, the InAs layer coagulates into small three-dimensional islands (on top of an InAs wetting layer) in order to achieve a better energy balance between strain, interface energy, and surface energy. Recently, a quantitative understand-

* Corresponding author. Fax: +49-30-8413-5106.
E-mail address: jacobi@fhi-berlin.mpg.de (K. Jacobi)

0039-6028/99/$ – see front matter
PII: S0039-6028(99)00713-X

ing of the self-assembly of quantum dots was achieved by Pehlke et al. [2]. When breaking up into dots, the strain energy stored in the film becomes reduced at the expense of creating surfaces for the dots. InAs surface energies were computed ab initio for several orientations, and the elastic energy of the islands was calculated within a continuum theory [2]. The resulting equilibrium islands are bounded by {110}, {111}, and $\{\bar{1}\bar{1}\bar{1}\}$ facets and a (001) surface on top. An important input to these calculations was the (reasonable) assumption that only the low-index surfaces determine the cluster morphology. Although reasonable, this assumption has to be proven further. Experimentally, this represents a very difficult task. From transmission electron micrographs, for example, it has not been possible so far to determine whether a pyramidally shaped cluster is capped or not and whether or not the edges are rounded by high-index surfaces.

A priori, it is not evident that only low-index surfaces contribute to the morphology of quantum dots. Instead, it may be necessary to take high-index surfaces into consideration as we will show in the following. For example, it has already been found that GaAs(113) exhibits a stable (8×1)-reconstructed surface [3–6]. According to our analysis, its surface energy is rather low, establishing it as a good candidate to contribute to the assemblage of quantum dots [7]. Moreover, we expected that GaAs(112)A and $(\bar{1}\bar{1}\bar{2})$B surfaces may be of a similar quality. Fig. 1 depicts a ball-and-stick model of the bulk-truncated GaAs(112)A and $(\bar{1}\bar{1}\bar{2})$B surfaces. From the side view (Fig. 1b), it is evident that the {112} planes contain an equal number of Ga and As atoms, i.e., they are nonpolar. Nevertheless, the A side differs from the B side. The A (B) side contains one threefold-coordinated Ga (As) atom in the first layer and one in the second layer, and one twofold-coordinated As (Ga) atom in the first layer. Fig. 1b also shows that the bulk-truncated {112} surfaces consist of two-atomic-rows wide {111} terraces and one {100}-like step parallel to the $[1\bar{1}0]$ direction. Thus, the question was whether, from this simple starting point, a low-energy, somehow reconstructed GaAs{112} surface could be found. We will show below that this is not the case even under MBE preparation and in-situ analysis.

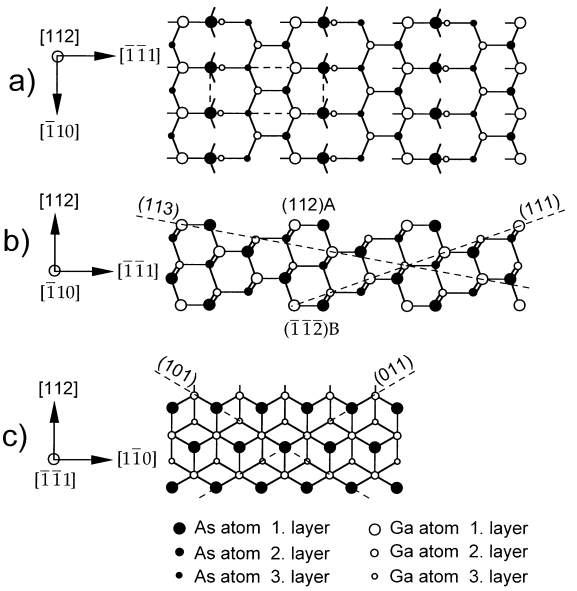

Fig. 1. Ball-and-stick model of the ideal, bulk-truncated GaAs{112} surface: (a) top view for the GaAs(112)A surface; (b) side view, cut along the $(1\bar{1}0)$ plane exposing a cut trough the (112)A surface (top) and, the $(\bar{1}\bar{1}\bar{2})$B surface (bottom); (c) side view, cut along the $(\bar{1}\bar{1}1)$B surface.

Only few contributions deal with GaAs{112} so far. This is certainly due to the early observation that this surface is not stable but facets. Ranke [8] found by LEED on a cylindrically shaped crystal, prepared by ion bombardment and annealing (IBA), that the $(11\bar{2})$B surface (which belongs to the $\{\bar{1}\bar{1}\bar{2}\}$B planes) facets into $(10\bar{1})$ and $(01\bar{1})$ planes which are inclined by $\pm30^\circ$ with respect to the $(11\bar{2})$B surface (see Fig. 1c). Hren et al. [9] studied IBA prepared GaAs(112)A and $(\bar{1}\bar{1}\bar{2})$B surfaces by LEED. Both A and B faces formed {110} facets 50–100 Å in size. The facets were inclined by 30 and 54° against the (112)A plane. Unfortunately, these authors could not differentiate between A and B faces. Also, we should note here that IBA is not appropriate to prepare As-rich GaAs surfaces [10].

Nötzel et al. [11] studied the MBE prepared GaAs(112)A surface by reflection high-energy electron diffraction (RHEED). They observed a reversible transition from a flat but disordered surface below 550°C to a faceted surface above 590°C. On the latter, asymmetric pyramids of

2.3 Å height are formed out of {110}, 6.9 Å wide {111} and 4 Å wide {100} facets. These structures are remarkably small with dimensions of only one to two lattice constants. The authors claim that these 'microstructures' are regularly arranged over larger areas, the diameter of which was estimated to be 70 Å. A minimum domain of the order of 100 Å is necessary in order to achieve some diffracted electron intensity in RHEED. We will show that our results do not support the findings of Nötzel and coworkers.

In this contribution, we report on the morphology of the GaAs(112)A and $(\bar{1}\bar{1}\bar{2})$B surfaces after MBE preparation. On both surfaces, strong faceting is observed, consisting of inverted-pyramid-like depressions with four or five facets of {110}, (111), and $(\bar{1}\bar{1}\bar{1})$, $(\bar{1}\bar{1}\bar{3})$, and {124} orientation forming the side walls. The dimension of these structures is of the order of 200 nm and below. We will show that the faceting is well understood in terms of surface energies from ab-initio calculations. Some of our results have already been presented in short conference papers [12,13] and in a contribution on the importance of high-index surfaces for the morphology of GaAs quantum dots [7]. In this contribution, we present all our results in a complete and consistent manner and draw final conclusions from our combined experimental and theoretical investigation. The paper is organized as follows: the data for GaAs(112)A and $(\bar{1}\bar{1}\bar{2})$B are presented in Section 3, calculated surface energies are presented in Section 4, and the results are discussed in Section 5.

2. Experimental

The experiments were performed in a set-up of three ultra-high vacuum (UHV) chambers connected by UHV-transfer lines and a load lock. The analysis chamber had a base pressure of 5×10^{-11} mbar and the MBE and the STM chamber one of 1×10^{-10} mbar. The MBE chamber contained two solid source MBE cells, a cooling shield, a 3 kV RHEED system and a movable ion gauge for measuring the pressure within the As_4 and Ga beams [beam equivalent pressure (BEP)]. During growth, the samples were heated by thermal radiation from a filament positioned at the backside of the sample holder, and the temperature was monitored with a pyrometer.

The analysis chamber was equipped with an Ar^+ ion gun, a mass spectrometer, a LEED optics and an angle-resolved photoelectron spectrometer (ADES400, VG). The system of the MBE and analysis chamber was designed for use with a He discharge lamp in the laboratory or at the toroidal grating monochromator4 (TGM4) beam line of the Berlin synchrotron radiation facility BESSY (Berliner Elektronenspeicherring-Gesellschaft für Synchrotronstrahlung). The surface core-level spectra were measured with an angle of incidence of light of 45° with respect to the surface normal.

For STM, we used a commercially available instrument (VP2, Park Scientific Instruments) mounted in a third small UHV chamber and connected to the other chambers by an additional UHV-transfer line. This instrument was adapted to our requirements [14]. Images were acquired in constant-current mode with tunneling currents between 0.2 and 0.3 nA and sample biases between -2 and -3 V.

The samples were of size $10\times10\times0.5$ mm^3. The (112)A sample was from an n-type wafer (AXT, Si doped, epiready). The $(\bar{1}\bar{1}\bar{2})$B sample was provided by Y.R. Xing [15]. For the STM work on $(\bar{1}\bar{1}\bar{2})$B, we used a wafer from Wafer Technology (Si, $6.3\text{–}34\times10^{17}$ cm^{-3}). The samples were degreased with propanol and fixed by a small droplet of liquid In to the sample holder made of Ta. The samples were then introduced into the UHV via the load lock, degassed for about 12 h at 250°C, sputtered with 1 kV Ar^+ ions for 45 min and annealed at 500°C in As_4 for about 30 min. During MBE growth, substrate temperatures between 450 and 600°C and As_4:Ga BEP ratios between 5 and 30 were chosen. In order to avoid As excess following growth, the sample temperature was held at 500°C until the As_4 pressure dropped below 2×10^{-9} mbar. At a growth rate of about 0.2 Å/s, GaAs layers of 50–100 nm thickness were grown.

The surfaces prepared were studied by spot profile analysis LEED or STM in the laboratory or with LEED and photoelectron spectroscopy at BESSY. Several typical samples were brought to

air and analyzed using an atomic force microscope (AFM) or scanning electron microscope (SEM).

3. Results and discussion

3.1. LEED results for GaAs(112)A

Surprisingly, GaAs(112)A could not be prepared as an atomically flat surface; instead, it faceted independently of growth parameters during MBE growth. A spot profile analysis LEED pattern is shown in Fig. 2. Depending on the primary electron energy, the spots are split into five facet spots. One such group of spots is shown in Fig. 2b. In the center of the group, a single spot is expected for a flat GaAs(112)A surface. In fact, the intensity is very small there, indicating that the whole (112)A surface is broken up into facets leaving only vanishing small parts oriented parallel to (112)A. By varying the primary energy, the azimuthal motion direction of the facet spots can be followed, and the angles between the facet planes and the ideal (112)A surface can be deduced. In this way, the facets can be identified as (101), (011), (111), (124), and (214) planes, as indicated by the different spots in Fig. 2b. From this LEED pattern, we concluded in our earlier publication [12] that the surface breaks up into a mixture of roof like structures containing (101) and (011) planes with the ridge pointing along $[11\bar{1}]$ and asymmetric triangular pyramids made of (111), (124) and (214) planes. Later, we found out that this model is too simple, and we will show below that the real structure can be recognized from the AFM, SEM and STM images.

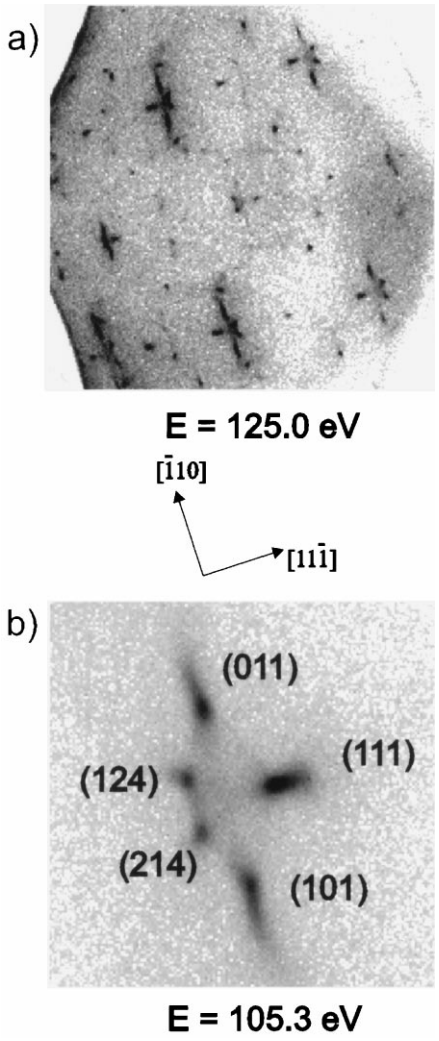

Fig. 2. Spot-profile-analysis low-energy electron diffraction (SPA-LEED) pattern of the GaAs(112)A surface. The primary electron energy, E, is indicated: (a) overview; (b) the (0,0) beam; the orientation of the facets is indicated (see text). From Ref. [12].

3.2. SEM, AFM and STM images of GaAs(112)A

Fig. 3 shows SEM images taken after transfer of the sample through air. The surface is densely covered by a rather irregular structure extending over the whole surface of which Fig. 3a shows a $7.1 \times 4.7\ \mu m^2$ sector. The AFM image of Fig. 4a, taken under approximately the same magnification of 1.3×10^4 as the SEM image in Fig. 3, shows some similarly resolved structures of the same size. It can be seen that the structures consist of depressions. This could not be concluded from the SEM analysis. The image gives the impression of structures with a rectangular base. In Fig. 4b, one of those structures is depicted at a magnification further enlarged by a factor of 20. Careful inspection reveals an internal structure indicated by broken lines in Fig. 4b. It can be seen that the depression is formed by the use of five different facets which correspond well with the SPA-LEED

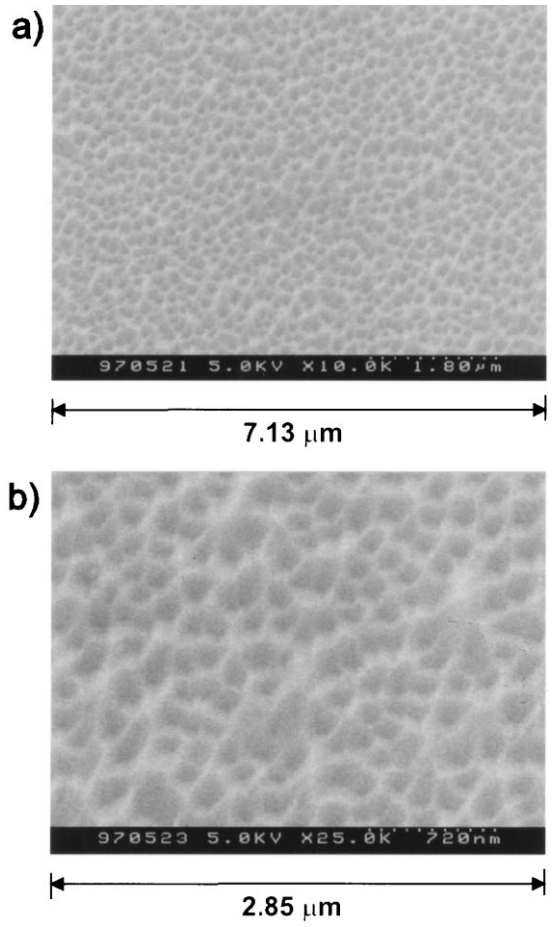

Fig. 3. Ex-situ scanning electron microscope (SEM) images of the GaAs(112)A surface.

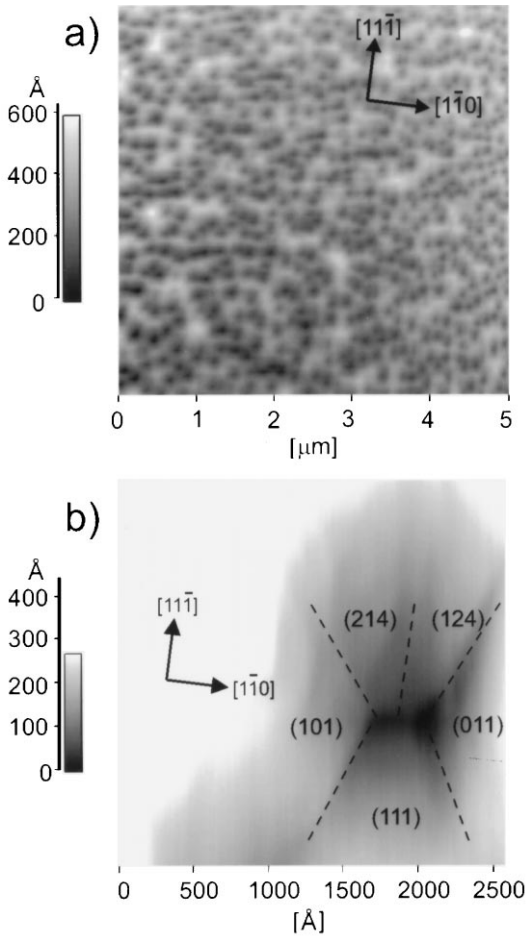

Fig. 4. Ex-situ atomic-force microscope (AFM) images of the GaAs(112)A surface. The length scales are given on the *x*-axis. The facets, as derived from the SPA-LEED pattern, are indicated by broken lines in (b).

pattern. From the AFM images, it can be concluded that only one kind of structure is found that covers the whole surface and with a morphology that corresponds with the SPA-LEED observation.

Recently, improvements in the experimental set-up enabled in-situ STM images to be collected [13]. Fig. 5 shows a typical STM image. Even more details of the depressions can be seen. The (111) facet starts with a straight line, and the base of the (214) and (124) facets clearly points towards the lower right corner of Fig. 5, i.e. into the [11$\bar{1}$] direction. From these large-area STM images, we extracted the angles with the horizontal [i.e. the nominal (112)A] plane for the different facets. The results are listed in Table 1. The observed trend is in agreement with the model indicated by broken lines in Fig. 4b, although there are also large deviations especially for the {110} facets. The reason is not clear at the moment.

3.3. Surface core-level shifts for GaAs(112)A

The analysis of surface core-level shifts (SCLSs) is a well-established technique for extracting information on the local bonding configuration of surface atoms. It is well known that surface atoms rearrange themselves in order to lower the surface

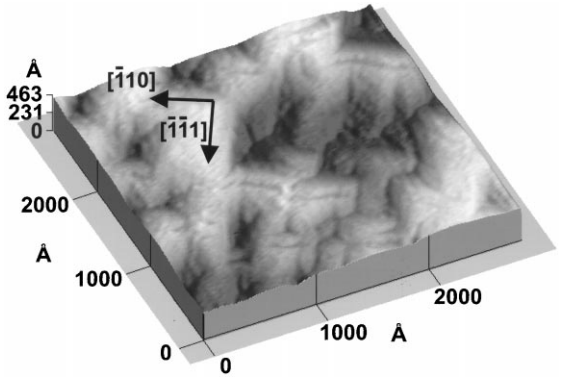

Fig. 5. Scanning tunneling microscope (STM) image of the GaAs(112)A surface. Tunneling current 0.2 nA, sample bias −2.0 V. From Ref. [13].

energy, which is largely increased by the formation of one to two broken bonds per surface atom during surface generation. There are a number of typical SCLSs known especially for the III–V compound semiconductor surfaces [16].

Fig. 6 shows spectra of the As 3d and Ga 3d core levels measured at normal emission for GaAs(112)A. The spectra were interpreted by fitting Voigt profiles to the measured data. The instrumental resolution (0.2 eV) is significantly better than the observed line width, which has a typical full width at half maximum (FWHM) of 0.5–0.6 eV. Each curve is decomposed into two spin-orbit doublets, one resulting from the bulk contribution (B) and the other from the surface (S1, S2). The best fits were obtained with a $3d_{3/2}$-peak to $3d_{5/2}$-peak intensity ratio of 0.66, which is the theoretical value of 2:3, and a spin-orbit split of 0.46 and 0.69 eV for the Ga 3d and

Table 1
Angles between facet planes and the nominal surface as derived from the model and from the STM images (experimentally)

GaAs(112)A					
Facet plane	(101)	(011)	(111)	(214)	(124)
Model angle (°)	30	30	19.5	11.5	11.5
Experimental angle (°)	14	15	14	12	10
GaAs($\bar{1}\bar{1}\bar{2}$)B					
Facet plane	(0$\bar{1}\bar{1}$)	($\bar{1}$0$\bar{1}$)	($\bar{1}\bar{1}\bar{1}$)	($\bar{1}\bar{1}\bar{3}$)	
Model angle (°)	30	30	19.5	10	
Experimental angle (°)	23	22	23	16	

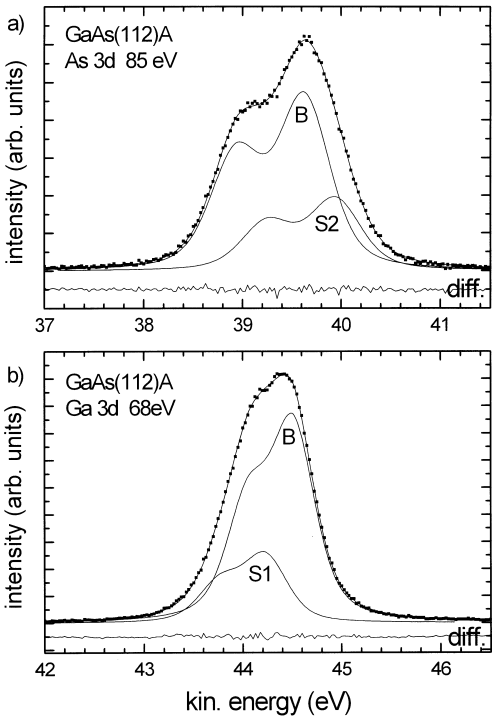

Fig. 6. Core-level spectra of As 3d at a photon energy $h\nu = 85$ eV (a) and Ga 3d at $h\nu = 68$ eV (b) for the GaAs(112)A surface. The filled squares are the measured data after background subtraction. The line is the fit assuming surface components S and a bulk component B. The difference (diff.) between the data and fit is also given. From Ref. [12].

the As 3d emission, respectively. The spin-orbit split values are in very good agreement with the literature data [17]. As is known for spectroscopy of SCLSs, the decomposition shown in Fig. 6 is strongly supported by the width of the bulk component that can be measured, for example, at smaller photon energies when the kinetic energy of the photoelectron is smaller and the escape depth larger due to the larger mean free path for inelastic scattering. This remark also concerns the decomposition of the spectra of GaAs($\bar{1}\bar{1}\bar{2}$)B in Section 3.6 (Fig. 11).

The surface component of As (Ga) is shifted by 0.31 eV (−0.28 eV) to a higher (lower) kinetic energy with respect to the bulk component. A shift to a higher kinetic energy means a shift to a lower binding energy. From the established interpretation of SCLSs collected from low-index GaAs

Table 2
List of the Ga 3d and As 3d surface core-level shifts (in units of eV) of GaAs(112)A and $(\bar{1}\bar{1}\bar{2})$B

		GaAs(112)A	GaAs$(\bar{1}\bar{1}\bar{2})$B
Ga 3d	S1	−0.28	−0.23
	S2	–	–
As 3d	S1	–	−0.59
	S2	+0.31	+0.48

surfaces, we assign the As surface component to threefold-coordinated As atoms with one lone pair, which appears both on the (110) surface and on the (2×2) reconstruction of the (111)A surface. The Ga surface component is associated with Ga atoms with one empty dangling bond on the (110) surface and several Ga 'rest atoms' on the (111)A-(2×2). The existence of only one contribution in both cases and the position and relative intensity of the surface components are in agreement with other photoemission data from (111)A [18–20] and (110) [17,18,20] surfaces. {124} surfaces have so far not been investigated separately. Our results suggest that they should also have surface components shifted into the directions observed here for GaAs(112)A. A summary of the shifts is listed in Table 2.

3.4. LEED results for GaAs$(\bar{1}\bar{1}\bar{2})$B

Two SPA-LEED patterns of GaAs$(\bar{1}\bar{1}\bar{2})$B are shown in Fig. 7. Similar to (112)A, the surface is highly faceted following MBE preparation. In Fig. 7b, the area of one single spot (the 0,0 beam) is depicted. The facet orientation, as deduced in a similar way as for the (112)A face, is indicated. There is no coherently diffracted intensity in the center of the pattern, indicating that no ordered nominal $(\bar{1}\bar{1}\bar{2})$B surface is left over contributing to the LEED pattern. Opposite (112)A, the surface breaks up into structures with four different facets: two $\{0\bar{1}\bar{1}\}$, $(\bar{1}\bar{1}\bar{1})$, and $(\bar{1}\bar{1}\bar{3})$. As we will see from the imaging techniques, these facets form the side walls of a single kind of depression that covers the surface.

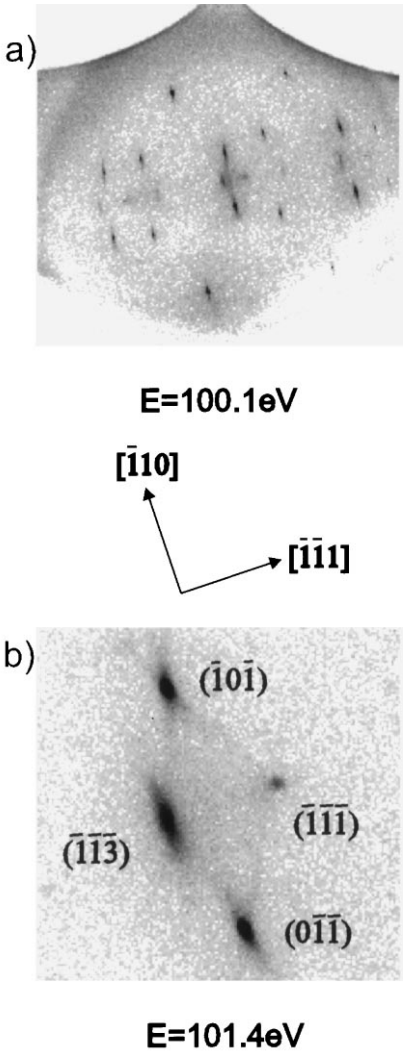

Fig. 7. Spot-profile-analysis LEED pattern of the GaAs$(\bar{1}\bar{1}\bar{2})$B surface. The primary electron energy is indicated. (a) overview, (b) (0,0) beam; the orientation of the facets is indicated (see text). From Ref. [12].

3.5. SEM, AFM and STM images of GaAs$(\bar{1}\bar{1}\bar{2})$B

In order to explore the morphology of the faceted surface, we employed three imaging techniques. Fig. 8 shows SEM images at slightly different magnifications. Rectangular shaped features can be seen, for which we have indicated the side wall indices. The largest facets extend up to 400 nm in the $[\bar{1}\bar{1}\bar{1}]$ direction and 200 nm in the

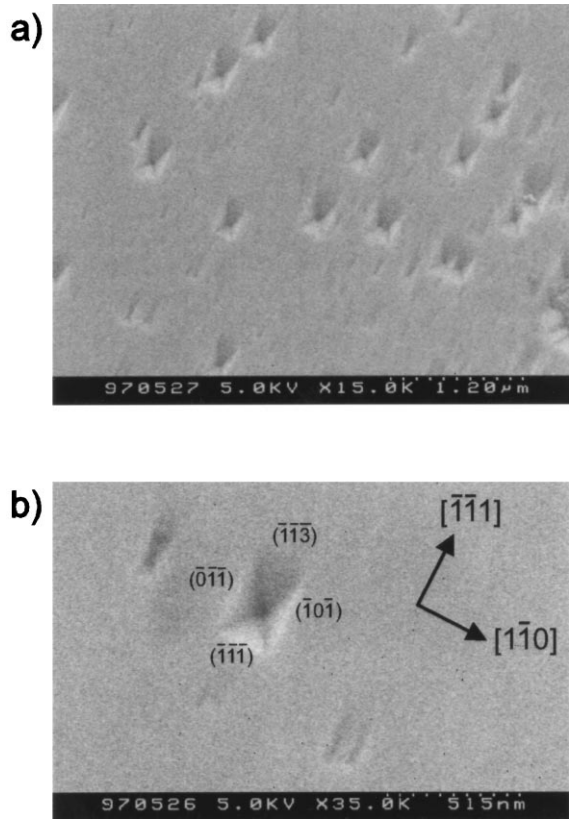

Fig. 8. Ex-situ scanning electron microscope (SEM) images of the GaAs($\bar{1}\bar{1}\bar{2}$)B surface. In (b) the facets, as derived from the SPA-LEED pattern, are indicated.

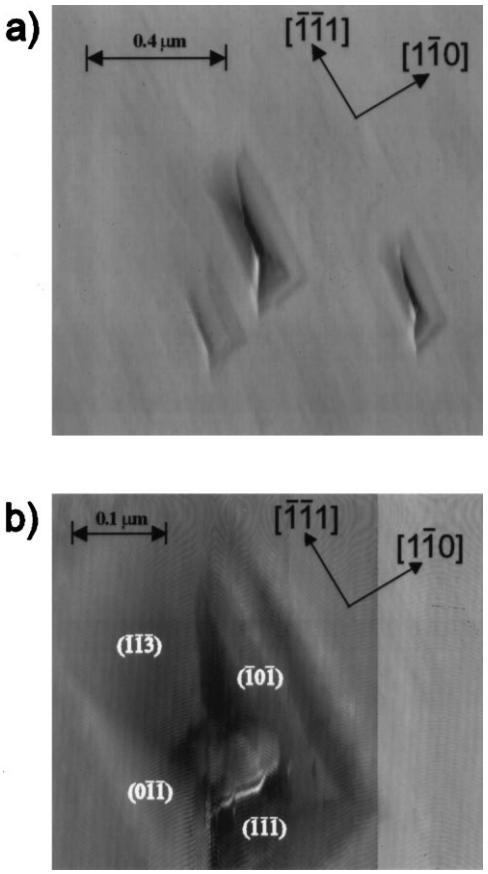

Fig. 9. Ex-situ atomic-force microscope (AFM) images of the GaAs($\bar{1}\bar{1}\bar{2}$)B surface. In (b) the facets, as derived from the SPA-LEED pattern, are indicated.

[1$\bar{1}$0] direction. The lateral separation of the features seen in Fig. 8 is rather large in contrast to that found for the (112)A face. In view of the STM picture shown below, we believe that there is a rather wide size distribution. Due to oxidation in air, the smaller structures may have been lost in the background.

The AFM images (Fig. 9) show the four facets of the structures with a better resolution. Knowing the relative orientation with respect to the wafer edge, the crystallographic orientation of the facets can be assigned. From the AFM images, the observed structures appear to consist of depressions. From Fig. 9, it becomes clear that the AFM tip is not able to resolve the deepest level of the hole, i.e. the tip of the inverted pyramid.

The large-area STM image (Fig. 10) resolves the orientation and morphology of the faceted

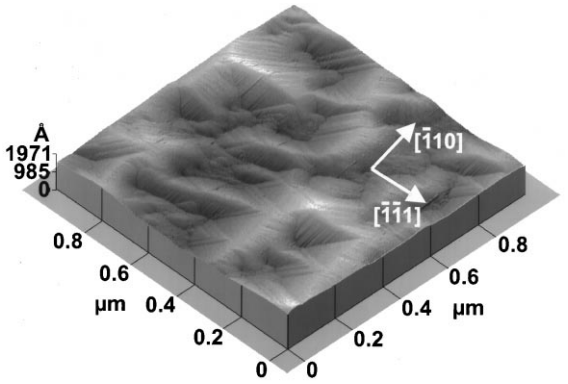

Fig. 10. Scanning tunneling microscope (STM) image of the GaAs($\bar{1}\bar{1}\bar{2}$)B surface. Tunneling current 0.2 nA; sample bias −2.0 V. From Ref. [13].

surface fairly well. We note that the dimensions of the depressions are about twice as large on the $(\bar{1}\bar{1}\bar{2})$B surface than on the (112)A surface. The STM image is in very good agreement with the SPA-LEED result but is somewhat different to the AFM image since the whole surface is covered by depressions that even partly interpenetrate each other, whereas in the AFM image, mostly isolated structures have been observed. This difference seems to be too large to be accounted for by the oxidation process during exposure to air; instead it may be also due to differences in parameters during MBE preparation. Such differences may introduce a difference in size distribution. From our STM study, we found that a more As-rich condition favors smaller structures. We will return to this point in Section 5.

3.6. Surface core-level shifts for GaAs($\bar{1}\bar{1}\bar{2}$)B

Fig. 11 shows the As 3d and Ga 3d SCL spectra of the GaAs($\bar{1}\bar{1}\bar{2}$)B surface measured at normal emission. The best fits are achieved for an intensity ratio of the $3d_{3/2}$-peak to the $3d_{5/2}$-peak of 0.67 (0.65) and a spin-orbit split of 0.45 eV (0.70 eV) for the Ga 3d (As 3d) spectrum. The Ga spectrum is decomposed into two doublets, one resulting from the bulk (B) and the other from the surface (S1), the latter being shifted by -0.23 eV to a higher binding energy (a smaller kinetic energy in Fig. 11). From our studies of low-index GaAs surfaces and in agreement with values from the literature, we assign this contribution to threefold-coordinated Ga atoms with one empty dangling bond. The direction and the amount of this shift are in agreement with the results on GaAs(110) [17,18,20] and GaAs($\bar{1}\bar{1}\bar{3}$)B [6] surfaces, which contain threefold-coordinated Ga atoms at the surface. For the GaAs($\bar{1}\bar{1}\bar{3}$)B surface, two surface contributions should exist [6]: one shifted to the higher binding energy side, and the other shifted to the lower binding energy side. However, in the spectra in Fig. 11b, only one surface contribution could be observed. This can be understood by the substantially smaller intensity of the second surface doublet present in the 3d spectra in Ref. [6] and the small coverage of the ($\bar{1}\bar{1}\bar{2}$)B surface with ($\bar{1}\bar{1}\bar{3}$) facets. The SCL spectra of As 3d show two

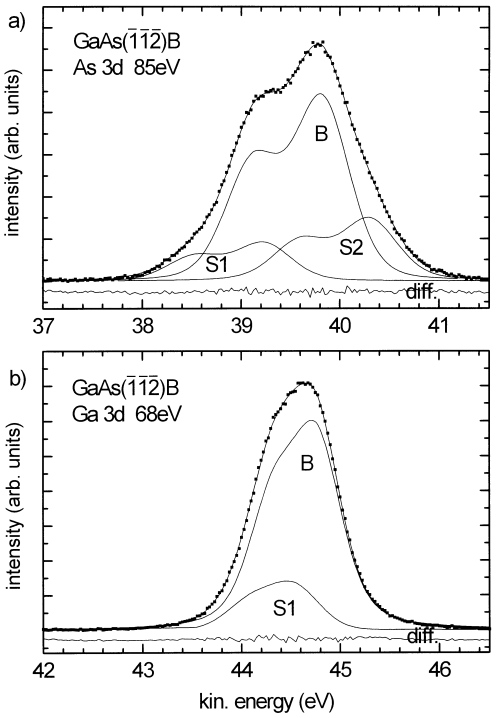

Fig. 11. Core-level spectra of As 3d at a photon energy $h\nu = 85$ eV (a) and Ga 3d at $h\nu = 68$ eV (b) for the GaAs($\bar{1}\bar{1}\bar{2}$)B surface. The filled squares are the measured data after background subtraction. The line is the fit assuming surface components S and a bulk component B. The difference (diff.) between the data and fit is also given.

differently coordinated As surface atoms. From the low-index GaAs surfaces, it is well known that the contribution S2, shifted by 0.48 eV to a higher kinetic energy (lower binding energy), is provided by threefold-coordinated As atoms with one lone pair or by As dimers [6,17,19,21]. Due to the occurrence of threefold-coordinated As atoms with one lone pair on all four facet planes [($\bar{1}0\bar{1}$), ($0\bar{1}\bar{1}$), ($\bar{1}\bar{1}\bar{1}$), and ($\bar{1}\bar{1}\bar{3}$)] we believe that this doublet originates from this kind of surface As atom. The second surface contribution (S1), which is found on the higher binding energy side (-0.59 eV), is assigned to extra absorbed As on As atoms or to As trimers on the GaAs($\bar{1}\bar{1}\bar{1}$)B surface [19,21]. These As atoms are only bonded to further As atoms, the bond being similar to that of As atoms in amorphous As. This result is in agreement with other photoemission data for the (110) [17,18],

$(\bar{1}\bar{1}\bar{1})$B [19,21] and for $(\bar{1}\bar{1}\bar{3})$B [6,18] surfaces. With these explanations, the surface contributions of the Ga 3d and As 3d core-level spectra can be attributed to the observed facet planes, which are {110}, $(\bar{1}\bar{1}\bar{1})$ and $(\bar{1}\bar{1}\bar{3})$ and agree well with the morphology of the $(\bar{1}\bar{1}\bar{2})$B surface as deduced from the imaging techniques. The intensity of the As S2 component is higher than expected for the estimated part of the surface covered by the $(\bar{1}\bar{1}\bar{1})$B and $(\bar{1}\bar{1}\bar{3})$B facets. It may indicate additional As_2 molecules adsorbed at the surface from the background pressure before transfer to the photoemission chamber.

4. Calculation of GaAs(112)A and $(\bar{1}\bar{1}\bar{2})$B surface energies

There has been much success in calculating surface structures of low-index GaAs surfaces using ab-initio total-energy methods [22]. The stable surface reconstruction is the one with the lowest surface free energy $\gamma_{\text{surface}}A$ of the surface area, A. Since GaAs consists of two elements, the difference in the number of the two species at the surface is an additional degree of freedom in the calculation. For this purpose, the surface is thought to exchange atoms of type i with a reservoir characterized by a chemical potential, μ_i. At zero temperature and zero pressure, the surface free energy is given by:

$$\gamma_{\text{surface}}A = E_{\text{surface}} - \mu_{\text{Ga}}N_{\text{Ga}} - \mu_{\text{As}}N_{\text{As}}, \tag{1}$$

where E_{surface} is the total surface energy, and N_i the number of the atoms of the ith species. The value of the chemical potential can vary in thermodynamical equilibrium only over a certain range. This range is fixed by two criteria:

1. the equilibrium between the crystal phase and the reservoir, that is, the chemical potential of each species must be the same in all the phases that appear in the total system:

$$\mu_{\text{Ga}} + \mu_{\text{As}} = \mu_{\text{GaAs}}^{\text{crystal}}. \tag{2}$$

2. all species are in phases corresponding to the minimal free enthalpy, in our case:

$$\mu_{\text{As}} \le \mu_{\text{As}}^{\text{crystal}}; \quad \mu_{\text{Ga}} \le \mu_{\text{Ga}}^{\text{crystal}}. \tag{3}$$

In the experiment, two limiting situations occur: in one case, the surface is in equilibrium with excess Ga metal, and this is called the Ga-rich condition with a small relative beam equivalent pressure. The other extreme is an As-rich condition, and the surface is in equilibrium with the excess As.

From Eq. (2), we can eliminate μ_{Ga} in Eq. (1):

$$\gamma_{\text{surface}}A = E_{\text{surface}} - \mu_{\text{GaAs}}N_{\text{Ga}} - \mu_{\text{As}}(N_{\text{As}} - N_{\text{Ga}}). \tag{4}$$

$N_{\text{As}} - N_{\text{Ga}}$ denotes the stoichiometry of the surface. It determines the slope of the surface energy versus chemical potential. A consistent counting rule for the stoichiometry is used for all orientations following Chetty and Martin [23].

When the chemical potential is varied, different reconstructions with different surface stoichiometries become thermodynamically stable. Generally, it has been found in the experiments that all observed reconstructions on all studied surfaces are semiconducting. On non-polar sufaces, this is achieved by electron transfer from the partly filled Ga dangling bond to the partly filled As dangling bond at the surface. The result is an empty dangling bond Ga in the conduction band and a filled As dangling bond at the top of the valence band. This has implications for the hybridization of the surface atoms, which tends to become a planar sp^2 hybridization for Ga and an orthogonal s^2p^3 hybridization for As. For the polar surfaces, to achieve low-energy semiconducting surfaces, Ga or As atoms are added to, or removed from, the surface.

For the computations, the surface was represented by periodically repeated slabs. The surface energy was determined from the total energy E_{tot} of the slab. E_{tot} was calculated by using density-functional theory (DFT) with the local density approximation (LDA) for the exchange-correlation functional. For further details, we refer to Moll et al. [22], who performed similar calculations for the (100), (110), (111) and $(\bar{1}\bar{1}\bar{1})$ surfaces of GaAs.

The surface free energy was calculated for a variety of reasonable surface models summarized in Table 3. The results for the (112)A and $(\bar{1}\bar{1}\bar{2})$B

Table 3
Different models for the GaAs(112)A and $(\bar{1}\bar{1}\bar{2})$B surfaces for which surface energies have been calculated[a]

Name	Surface	Starting structure
(1×1)-α	{112}	Truncated bulk structure
(1×1)-β	(112)A [$(\bar{1}\bar{1}\bar{2})$]	As (1×1)-α but first layer As [Ga] removed
(1×1)-γ	{112}	As (1×1)-α but first layer As substituted by Ga
(1×1)-δ	{112}	As (1×1)-α but first layer Ga substituted by As
(1×1)-ϵ	{112}	As (1×1)-α but first and 2nd layer Ga substituted by As
(2×1)-α	(112)A [$(\bar{1}\bar{1}\bar{2})$]	As (1×1)-α plus As [Ga] dimer formation along [$\bar{1}$10]
(2×1)-β	$(\bar{1}\bar{1}\bar{2})$	As, (1×1)-β plus Ga dimer formation along [11$\bar{1}$]

[a] The starting structure is described, which was relaxed in the ab-initio calculations.

surfaces are presented in Fig. 12. In order to investigate their stability, we have calculated the surface energy for the faceted structures assembled according to Herring's construction combining the {110}, {111}, {100}, and {113} faces and using results from the literature [7,22]. From Fig. 12, it can be seen that faceting lowers the energy with respect to all considered surface structures. According to our calculations, the (112)A and $(\bar{1}\bar{1}\bar{2})$B surfaces facet in agreement with our experiments. Since the high-index facets (as {124}) have been neglected in the calculations, the theoretically predicted roof arrangements consisting of (111) and (113) planes or {110} planes may not reproduce the real stable structure. However, the important and pivoting point of the theoretical study is the prediction of faceting. In particular, the $(\bar{1}\bar{1}\bar{2})$B surface undergoes faceting and exhibits a roof-like structure consisting of {110} planes along the [$\bar{1}$11] direction under As-rich conditions and roofs consisting of $(\bar{1}\bar{1}\bar{1})$ and $(\bar{1}\bar{1}\bar{3})$ planes pointing along the [01$\bar{1}$] direction under Ga-rich conditions. At As-rich conditions both roof-like structures are of the same energy. Therefore, one could imagine that both are combined and form the inverted pyramids found in experiment. In analogy to $(\bar{1}\bar{1}\bar{2})$B, one would expect a similar combination of roof-like structures for the (112)A surface. Unexpectedly, the anticipated (113) facet splits into two {124} facets. This observation suggests further theoretical investigations because also other low-energy surfaces may have been neglected. This indicates the importance of the feedback between theory and experiments for such complex systems.

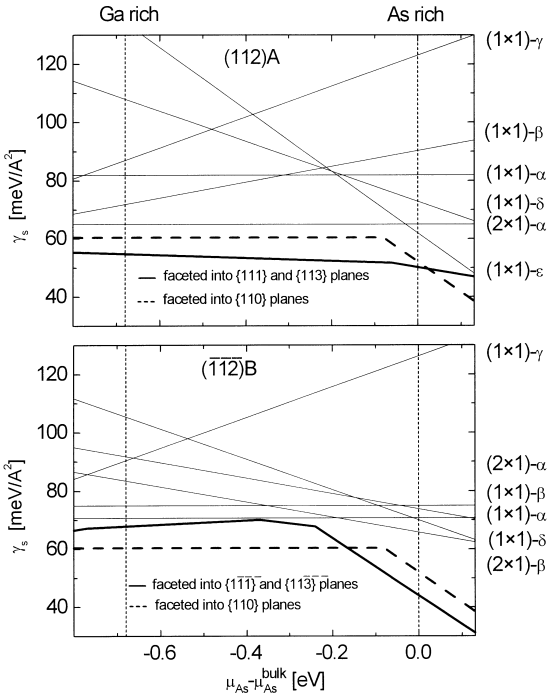

Fig. 12. Calculated surface energies, γ_S of the GaAs(112)A (upper part) and GaAs$(\bar{1}\bar{1}\bar{2})$B surface (lower part) as a function of the As chemical potential, μ_{As}. For the different models, see Table 3. From Ref. [7].

5. Discussion

For all parameters of vapor pressure and substrate temperature, tested during MBE growth, we

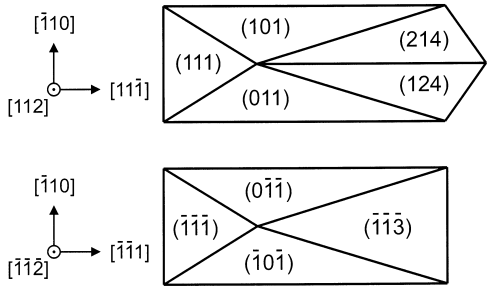

Fig. 13. Schematic sketches in top-view perspective of the depressions or inverted pyramids for the GaAs(112)A (top) and GaAs($\bar{1}\bar{1}\bar{2}$)B (bottom) surfaces.

found strong faceting on both GaAs(112)A and ($\bar{1}\bar{1}\bar{2}$)B surfaces. From STM and AFM, we found evidence that the surfaces are completely covered by a hole structure made of inverted pyramids. From the combination of SPA-LEED, STM, AFM and SCLSs, we were able to derive the models for these depressions as depicted in Fig. 13. The individual facets confine angles with the {112} surface of 30° for {110}, 15.5° {111}, 10.0° for {113}, and 11.5° for {124} leading to a surface enlargement by 15% {110}, 3.8% {111}, 1.5% {113}, and 2.0% {124} compared to the flat nominal {112} surface. It can be seen that the high-index surfaces are favored against {110} due to their smaller inclination with respect to {112}, which leads to a smaller increase of the surface during faceting. The main different lattice planes occurring as facets are also indicated in Fig. 1. The fraction by which the different facets contribute to the surface of the depression is given in Table 4. The relation between the different parts is approximately: {111}:{113} or {124}:{110} = 1:2:3. The angles between {112} and the different facets are important factors in the model calculations of Fig. 12.

If one takes into consideration the surface free energy calculated for the (113)A and ($\bar{1}\bar{1}\bar{3}$)B surfaces [7] the following can be deduced. For all As chemical potentials for which stable, i.e. low-energy, surfaces are found, the {111}/{113} roof reconstruction is lower in energy than the {110}/{110} roof. For (113)A, the (8×1) reconstruction was found to have the lowest energy throughout the whole As chemical potential range. For ($\bar{1}\bar{1}\bar{3}$)B, there is a so-called (1×1)-ζ reconstruction that is favored under As-rich conditions for which, in Fig. 12, the {($\bar{1}\bar{1}\bar{1}$}/{$\bar{1}\bar{1}\bar{3}$} roofs dominate.

Table 4
Contribution (%) of the different facets to the total surface of a single depression as shown in Fig. 13

Facet	{110}	{111}	{$\bar{1}\bar{1}\bar{3}$}	{124}
GaAs(112)A	49.7	14.7	–	35.7
GaAs($\bar{1}\bar{1}\bar{2}$)B	52.9	15.7	31.3	–

Clearly, the GaAs(112)A and ($\bar{1}\bar{1}\bar{2}$)B surfaces are not of a low energy in spite of their simple, bulk-truncated structure, as can be seen from Fig. 1. A closer view at the bulk-truncated structure makes this plausible. Looking along [1$\bar{1}$0], it consists of two rows of threefold-coordinated, {111}-like atoms and one row of twofold-coordinated, {100}-like atoms. The bulk-truncated GaAs(111)A and ($\bar{1}\bar{1}\bar{1}$)B surfaces are not of a low-energy, but exhibit a number of known reconstructions. However, the two (111)A-like rows at the (112)A surface, for example, would be able to rearrange into a row of (2×2) reconstructed unit cells of the Ga-vacancy model. The (100)-like, twofold-coordinated atom is of a high energy, which could be lowered by dimer formation in the [1$\bar{1}$0] direction. That this does not occur, may be due to the strain which is always connected with dimer formation. For (112)A, this strain is always directed along one direction and cannot be compensated by a patchwork-like ordering of patches along different strain directions.

It is interesting to compare the (112)A and (113)A surfaces. On the bulk-truncated (113)A surface, there is one row of threefold- and one row of twofold-coordinated atoms. Also, in this case, the twofold-coordinated atoms do not simply form dimers, resulting in a $\times2$ periodicity. Instead, the rather complicated 8×1 structure is formed with the $\times8$ periodicity along the [1$\bar{1}$0] direction [8]. Only every fourth possible As dimer is formed with a corrugation two layers deep in between. Although the bulk-truncated structure of (112)A seems as simple as (113)A, no low-energy structure could be found for (112)A. A similar argument can be made for the B faces.

Most remarkably, we observe the occurrence of

high-index surfaces contributing to the morphology of the depressions. This indicates that such surfaces, among them (113)A, $(\bar{1}\bar{1}\bar{3})$B and {124}, cannot be ignored when constructing the equilibrium crystal shape of GaAs and of GaAs quantum dots. Recent calculations [22] of the GaAs equilibrium crystal shape did not include {113} or {124} surfaces and should be reconsidered critically for this reason. We suppose that this argument probably holds also for other III–V quantum dots.

The importance of the GaAs{113} surface as a terminating face of low-dimensional quantum structures is demonstrated also in Ref. [24]. Kapon et al. prepared grooves at an AlAs(001) substrate by the lithography technique. In these grooves, GaAs quantum wires embedded in AlAs could be assembled. As shown by cross-sectional transmission electron microscopy (TEM), the side walls consists of {111} planes. At the transition from the (001) bottom to the {111} side walls, {113} surfaces are clearly observed in TEM.

Another interesting result in our investigation is the observation of {124} facets. The {124} surface is completely unexplored so far. Comparing the two depressions found at the (112)A and $(\bar{1}\bar{1}\bar{2})$B surfaces, as depicted in Fig. 13, one would expect a (113)A facet instead of the (214) and (124) facets, since for the (113)A surface, an 8×1 reconstruction has been found [3–6], which is of a low energy [7]. It is, therefore, remarkable that the anticipated (113) facets break up into {124} facets. The {124} facets seem to be of an even lower surface energy than (113)A. The difference seems to be of the order of 10% since the area contribution of this facet (113)A or {124}] rises from 31.3 to 35.7% (see Table 4 and Fig. 13). From the calculated surface free energies, we have derived upper limits of its surface energy with respect to (110), (111), and (113) [7]. It should be noted here that, so far, we have not dealt with contributions from edges and corners to the total energy, which may become important for the energy balance at this point. Thus, it could well be that {124} surfaces form ridges of a lower energy with {110} surfaces than (113)A surfaces do.

Also, for GaAs(112)A and $(\bar{1}\bar{1}\bar{2})$B, SCL spectroscopy turned out to be a helpful tool for structural evaluation. As can be seen from the comparison of the SCLS for the A and B side, there are large differences for the As 3d spectra. For the B side, there are two shifts, S1 and S2, whereas for the A side, there is only one shift, S2. The component S1 is quite typical for As bonded to As, as it is found in the As trimer bonded to three As surface atoms in the GaAs$(\bar{1}\bar{1}\bar{1})(2\times2)$ reconstruction. The S1 component is observed only at the B side for which we observed $(\bar{1}\bar{1}\bar{1})$ facets. However, we have to admit that we have not observed any S2 shift for Ga 3d, which we would expect for the $(\bar{1}\bar{1}\bar{3})$B(1×1) surface [6]. The energy half width of the fitted components is somewhat larger for the $(\bar{1}\bar{1}\bar{1})$B face, which may be locally less well ordered than the (112)A face, resulting in some additional inhomogeneous broadening.

Finally, there are remarkable differences in morphology between the A and B surfaces: The (113)A facet of the depressions on the (112)A surface decomposes into two {124} facets, i.e. the surface free energy is lowered further below the rather low value found for (113)A. Furthermore, the $(\bar{1}\bar{1}\bar{3})$B is stable only under As-rich conditions [7]. Therefore, we speculate that depressions on the (112)A surface are more stable than those on the $(\bar{1}\bar{1}\bar{2})$B surface. During growth, this could lead to a more effective Oswald ripening on the $(\bar{1}\bar{1}\bar{2})$B surface, i.e. the larger depressions grow at the expense of the smaller depressions. In fact, the lateral dimensions are larger by a factor of about two on the $(\bar{1}\bar{1}\bar{2})$B surface [13]. This may also explain that for the B face, only rather large depressions are observed in AFM and STM after transfer through air. The depressions on the A face may withstand reactions better in air, whereas the smaller depressions on the B face are attacked and smeared out by lateral mass transport in an amorphous mixed oxide phase.

6. Conclusion

Our investigation of the morphology of the faceted GaAs(112)A and $(\bar{1}\bar{1}\bar{2})$B surfaces revealed rather uniform depressions built from {110},

{111}, $(\bar{1}\bar{1}\bar{3})$ and {124} facets. This result was very well confirmed by model calculations, which showed that faceting into $(\bar{1}\bar{1}\bar{1})/(\bar{1}\bar{1}\bar{3})$ or {110}/{110} roof-like structures considerably lowers the surface free energy. Our observation indicates that high-index GaAs surfaces play a role in terminating low-dimensional quantum structures. Also, recent calculations [22] of the GaAs equilibrium crystal shape should be critically reconsidered since high-index surfaces were not included.

Our result is in accordance with the observations made for the GaAs(113)A surface. Although the bulk-truncated version of this surface is of a similar simplicity, the low-energy 8×1 reconstruction has turned out to be very complicated but very stable. Apparently, such a sophisticated solution does not exist for GaAs(112)A or $(\bar{1}\bar{1}\bar{2})$B. We could not reproduce the results of Nötzel et al. [11].

Finally, our results for the GaAs{124} surface suggest that it is of a low energy and should also be studied in the future.

Acknowledgements

We thank Peter Geng for technical support and Maria Richard for typesetting the manuscript and designing the figures. We acknowledge the help of the BESSY staff. The project was supported by the Bundesministerium für Forschung und Bildung under grant No. 05622EBA4 and by the Deutsche Forschungsgemeinschaft (Sonderforschungsbereich296, Projects A1, A2 and A5).

References

[1] N.N. Ledentsov, in: M. Scheffler (Ed.), 23rd Int. Conf. Physics of Semiconductors, Singapore (1996) p. 19.
[2] E. Pehlke, N. Moll, A. Kley, M. Scheffler, Appl. Phys. A65 (1997) 525.
[3] M. Wassermeier, J. Sudijono, M.D. Johnson, K.T. Leung, B.G. Orr, L. Däweritz, K. Ploog, Phys. Rev. B 51 (1995) 14721.
[4] R. Nötzel, N.N. Ledentsov, L. Däweritz, M. Hohenstein, K. Ploog, Phys. Rev. Lett. 67 (1991) 3812.
[5] C. Setzer, J. Platen, P. Geng, W. Ranke, K. Jacobi, Surf. Sci. 377–379 (1997) 125.
[6] C. Setzer, J. Platen, W. Ranke, K. Jacobi, Surf. Sci. 419 (1999) 291.
[7] J. Platen, A. Kley, C. Setzer, K. Jacobi, P. Ruggerone, M. Scheffler, J. Appl. Phys. 85 (1999) 3597.
[8] W. Ranke, Physica Scripta T4 (1983) 100.
[9] P. Hren, D.W. Tu, A. Kahn, Surf. Sci. 146 (1984) 69.
[10] W. Ranke, K. Jacobi, Prog. Surf. Sci. 10 (1981) 1.
[11] R. Nötzel, L. Däweritz, K. Ploog, Phys. Rev. B 46 (1992) 4736.
[12] J. Platen, C. Setzer, P. Geng, W. Ranke, K. Jacobi, Microelectr. J. 28 (1997) 969.
[13] L. Geelhaar, J.M. Márquez, K. Jacobi, A. Kley, P. Ruggerone, M. Scheffler, Microelectr. J. 30 (1999) 393.
[14] P. Geng, J. Márquez, L. Geelhaar, C. Setzer, J. Platen, K. Jacobi, Rev. Sci. Instrumen. (1980) submitted.
[15] Y.R. Xing, Institute of Semiconductors, Chinese Academy of Sciences, P.O. Box 912, Beijing 100083, P.R. China.
[16] S.M. Scholz, PhD thesis, Technische Universität Berlin, 1995.
[17] D. Eastman, T.-C. Chiang, P. Heimann, F. Himpsel, Phys. Rev. Lett. 45 (1980) 656.
[18] W. Ranke, J. Finster, H.J. Kuhr, Surf. Sci. 187 (1987) 112.
[19] J.M.C. Thornton, P. Weightman, D.A. Woolf, C.J. Dunscombe, Phys. Rev. B 51 (1995) 14459.
[20] C. Priester, G. Allan, M. Lannoo, Phys. Rev. Lett. 58 (1987) 1989.
[21] C. Setzer, J. Platen, H. Bludau, M. Gierer, H. Over, K. Jacobi, Surf. Sci. 402–404 (1998) 782.
[22] N. Moll, A. Kley, E. Pehlke, M. Scheffler, Phys. Rev. B 54 (1996) 8844.
[23] N. Chetty, R.M. Martin, Phys. Rev. B 44 (1991) 5568.
[24] E. Kapon, F. Reinhardt, G. Biasiol, A. Gustafsson, Appl. Surf. Sci 123–124 (1998) 674.